J. Fluid Mech. (1982), *vol.* 119, *pp.* 443–473
Printed in Great Britain

Subharmonics and vortex merging in mixing layers

By CHIH-MING HO AND LEIN-SAING HUANG
Department of Aerospace Engineering, University of Southern California, Los Angeles, California 90007, U.S.A.

(Received 11 March 1981 and in revised form 17 September 1981)

In the present study, it is shown that the spreading rate of a mixing layer can be greatly manipulated at very low forcing level if the mixing layer is perturbed near a subharmonic of the most-amplified frequency. The subharmonic forcing technique is able to make several vortices merge simultaneously and hence increases the spreading rate dramatically. A new mechanism, 'collective interaction', was found which can bypass the sequential stages of vortex merging and make a large number of vortices (ten or more) coalesce.

A deeper physical insight into the evolution of the coherent structures is revealed through the investigation of a forced mixing layer. The stability and the forcing function play important roles in determining the initial formation of the vortices. The subharmonic starts to amplify at the location where the phase speed of the subharmonic matches that of the fundamental. The position where vortices are seen to align vertically coincides with the position where the measured subharmonic reaches its peak. This location is defined as the merging location, and it can be determined from the feedback equation (Ho & Nosseir 1981).

The spreading rate and the velocity profiles of the forced mixing layer are distinctly different from the unforced case. The data show that the initial condition has a long-lasting effect on the development of the mixing layer.

1. Introduction

During the past decade, two important experiments have made major advances in the understanding of mixing layers. Within a wide range of Reynolds numbers, Brown & Roshko (1974) concluded that the large coherent vortical structures are the intrinsic features of a turbulent mixing layer. At about the same time, Winant & Browand (1974) showed that the growth of a mixing layer is governed by the pairing mechanism of these vortical structures. These two concepts, together with the observation of coherent structures in turbulent boundary layers (Kim, Kline & Reynolds 1971), changed the trend of thought about turbulence. Turbulence was always thought to be a random flow field which could be treated by a stochastic approach. After recognition of the dominant role of the coherent structures in a shear layer, it became evident that the traditional stochastic methods, either experimental techniques or theoretical analyses, were not capable of revealing completely the characteristics of the quasi-ordered coherent structures.

Kovasznay, Kibens & Blackwelder (1970) developed the concept of conditional sampling, which can distinguish and measure flow regions with different characteristics, e.g. turbulent and non-turbulent, from a predetermined threshold. This technique

provides a powerful tool for studying the coherent structures. Wygnanski & Fiedler (1970) explored in detail the flow properties in the turbulent zone of a mixing layer. Browand & Weidman (1976) used the amplitude and the phase measured from two hot-film probes as the threshold, and conditionally sampled the vortices undergoing a pairing process. They found that the pairing process was responsible for the transverse momentum transport, i.e. production of the Reynolds stress.

The concept of coherent structures poses a problem to the theoreticians, because it is difficult to model quasi-ordered structures, which are neither deterministic nor stochastic. Recently, the direct simulation of coherent structures has shown promising results with the development of fast numerical schemes. Corcos & Sherman (1976) examined the roll-up of a shear layer into a vortex. Acton (1976) used discrete vortex elements in modelling the shear layer, and investigated the pairing of coherent structures. Ashurst (1976) employed discrete vortices to study the mixing in a free shear layer. Knight (1979) studied the relationship between the fine-scale turbulence and the coherent structures. Riley & Metcalfe (1980) used a pseudo-spectral method to solve the Navier–Stokes equation in a mixing layer. They supplied very valuable information about the mixing layer, and could simulate the vortex-merging phenomenon found by Ho and Huang (1978).

The other approach is to study the free shear layer from a stability point of view. Michalke (1965) calculated the spatial stability of a parallel shear layer. His results indicate that the most amplified frequency and the amplification rate of the instability waves scale with the momentum thickness and the mean velocity. Kelly (1967) proposed a subharmonic-resonance mechanism that can feed energy to the subharmonics. It has been shown that the far-field noise radiation can be predicted by using a wave-like approach (Tam 1971; Merkine & Liu 1975). One should be cautious in using these results to explain the formation or the merging of coherent structures. The stability analyses are linear or weakly nonlinear calculations, whereas the evolution of coherent structures is well into the nonlinear regime. This point will be elaborated further in this paper.

Mixing layers are important in many practical applications, e.g. combustion, chemical lasers. Enhancement of the mixing of two fluids in the two streams can be very helpful in these applications. The coherent structures have been said to engulf fluid into the mixing layer. Large strain rates occur during the pairing process and the interface between the two fluids is increased. A greater interfacial area provides an increased molecular mixing. Hence mixing in a shear layer can be improved if the amalgamation of coherent structures can be promoted.

In the present paper, first, the visualization experiment is used to illustrate the novel subharmonic forcing method by which the number of coherent structures involved in each merging can be controlled. Afterwards, the relationship between the stability and the initial development of the coherent structures is identified. The roles of feedback and subharmonic resonance in vortex merging are examined. Finally, the downstream development of the mixing layer is surveyed.

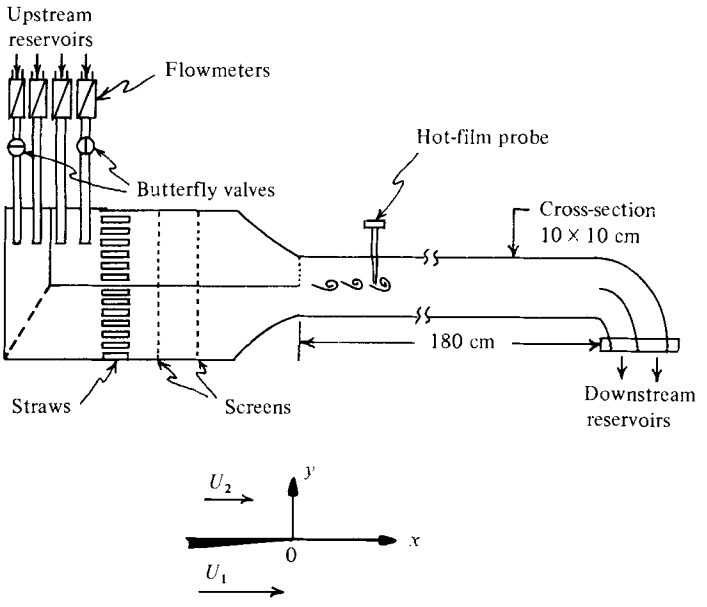

FIGURE 1. Experimental facilities.

2. Experimental facilities

The experiment was performed in a water channel (figure 1). The stagnation chamber is separated into two compartments by a splitter plate. The test section is connected to the stagnation chamber through a 9:1 contraction. The splitter plate ends with a sharp edge at the beginning of the test section. On the low-speed side of the contraction, a 60-mesh screen is placed about 3 mm in front of the trailing edge of the splitter plate such that the thickness of the boundary layer can be very much reduced. The wake, due to the two boundary layers, disappears at 1·5 cm. The cross-section of the test section is 10×10 cm and the length is 180 cm. Water is gravity-fed into the stagnation chamber from four upstream reservoirs. Four supply pipes connect the reservoirs to the stagnation chamber. The flow rates are controlled by four flowmeters (Fisher-Porter Type 10A3565AY). Two of the pipes have steady flows. Two butterfly valves are installed in the other two pipelines to provide velocity perturbations. The blades of the two valves are set 90° out of phase. The butterfly valves are driven by a DC motor. The amplitude and the frequency of the velocity perturbations can be varied by the combination of the flowmeters and the DC motor. Water is collected at the end of the test section and pumped back into the upstream reservoirs.

The velocity field is surveyed by hot-film probes (TSI Type 1210). The probes are mounted on a traverse with two degrees of freedom. The hot-film outputs are recorded on an analog tape recorder (Hewlett Packard Type 1040A) with frequency response up to 5 kHz. Signals are digitized and processed with a PDP 11/55 minicomputer.

The mixing layer is visualized with common food colouring injected on the surface of the splitter plate about 3 cm before the trailing edge on the low-speed side.

The origin of the Cartesian co-ordinates is located at the trailing edge of the splitter plate. The streamwise direction is the x-axis, and the vertical direction is the y-axis.

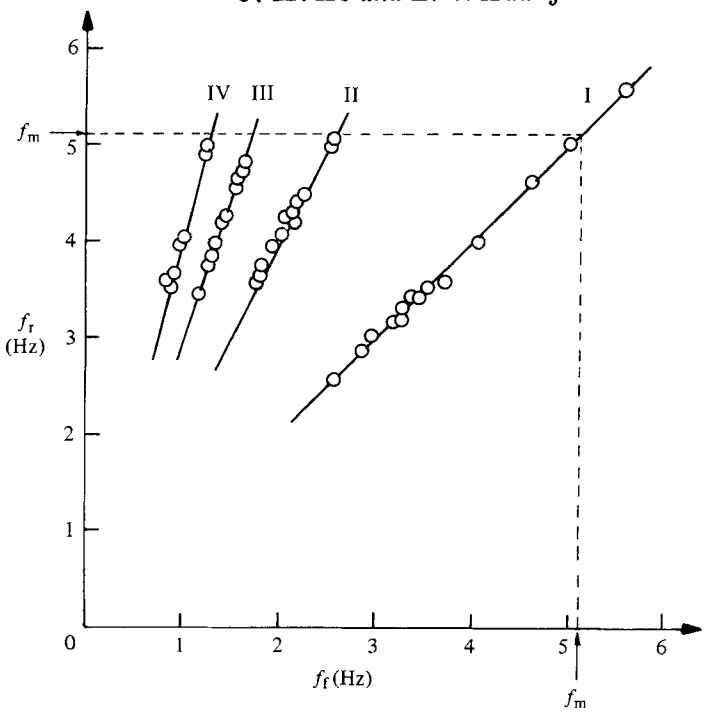

FIGURE 2. The response frequency *vs.* the forcing frequency.

3. Experimental results

3.1. *Visualization of the forced mixing layer*

3.1.1. *Response of a mixing layer under forcing.* In most of the test cases, the high-speed side of the mixing layer was kept at $U_1 = 9{\cdot}5$ cm/s, and the low speed was $U_2 = 5{\cdot}0$ cm/s. The vortices usually formed aperiodically in an unforced mixing layer, but there was a peak in the spectrum of streamwise velocity fluctuations. This peak frequency, referred to as the most-probable frequency f_m, was found to be 5·06 Hz, and close to the theoretical most-amplified frequency, designated by f_0 (see §3.2.1).

Forcing was provided by perturbing the flow rates of both streams of the mixing layer. Upstream of the trailing edge of the splitter plate, the velocity perturbations were in the streamwise direction only. Downstream of the trailing edge, transverse velocity perturbations appeared along with the streamwise velocity perturbations, because the curvature of the stagnation streamline must vary in time in order to accommodate the condition of continuity of pressure across the mixing layer. When the mixing layer is periodically forced, coherent structures develop periodically owing to the streamwise and transverse velocity perturbations.

The forcing frequency f_f was varied from 6·35 to 0·85 Hz, covering a range from somewhat higher than f_m to much lower than f_m. It was interesting to find that the instability frequencies (in the initial region) of the forced mixing layer were not necessarily the same frequency as f_f. The initially most-amplified instability frequency of the forced mixing layer was called the response frequency f_r, and was determined both by visualizing the passage of the vortices and by hot-film measurements 4 cm downstream from the trailing edge and upstream from any merging. The relationship between the response frequency and the forcing frequency is plotted in figure 2. The

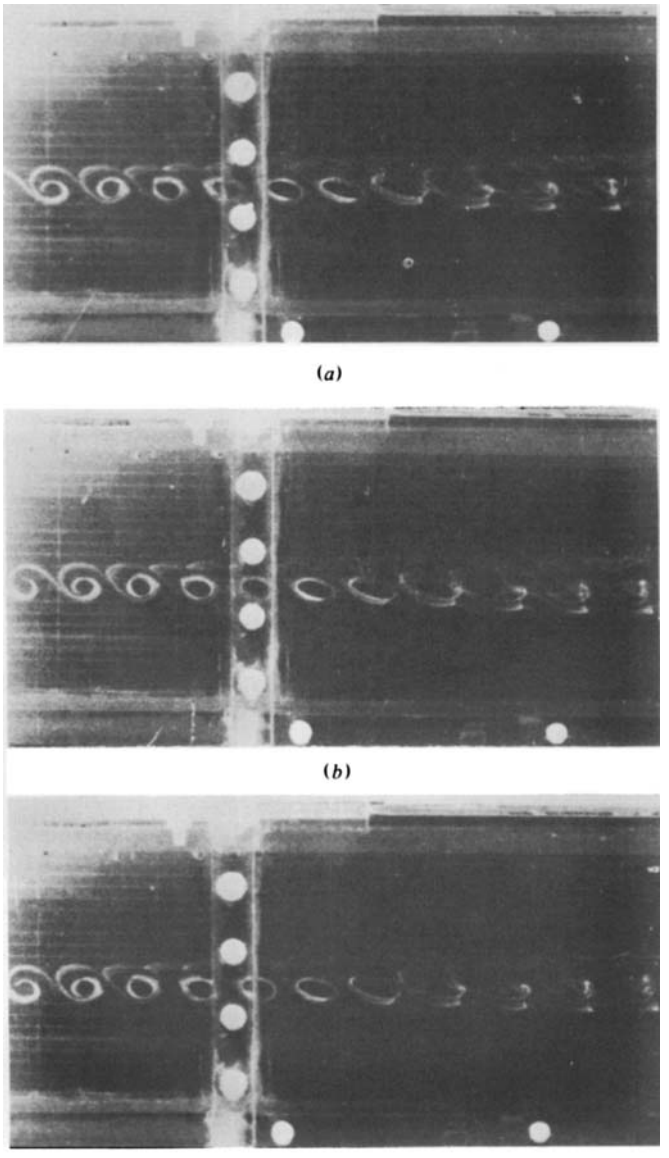

(*a*)

(*b*)

(*c*)

FIGURE 3. Mixing layer under mode I forcing; $f_f/f_m = 0{\cdot}70$, $\Delta\phi = 120°$.

results indicate that the vortices do not always form at the most-probable frequency f_m. When the forcing frequency is close to f_m the response frequency is the same as the forcing frequency. If the forcing frequency is below a certain limit the response frequency switches discontinuously to a higher frequency. In the present experiment, four frequency stages and discontinuities were found with decreasing forcing frequency. The frequency stages are designated as modes I, II, III, IV. Hysteresis is observed between stages.

3.1.2. *Vortex merging and collective interaction.* The evolution of the shear layer was visualized with a dye trace emerging from the trailing edge. When the mixing layer is

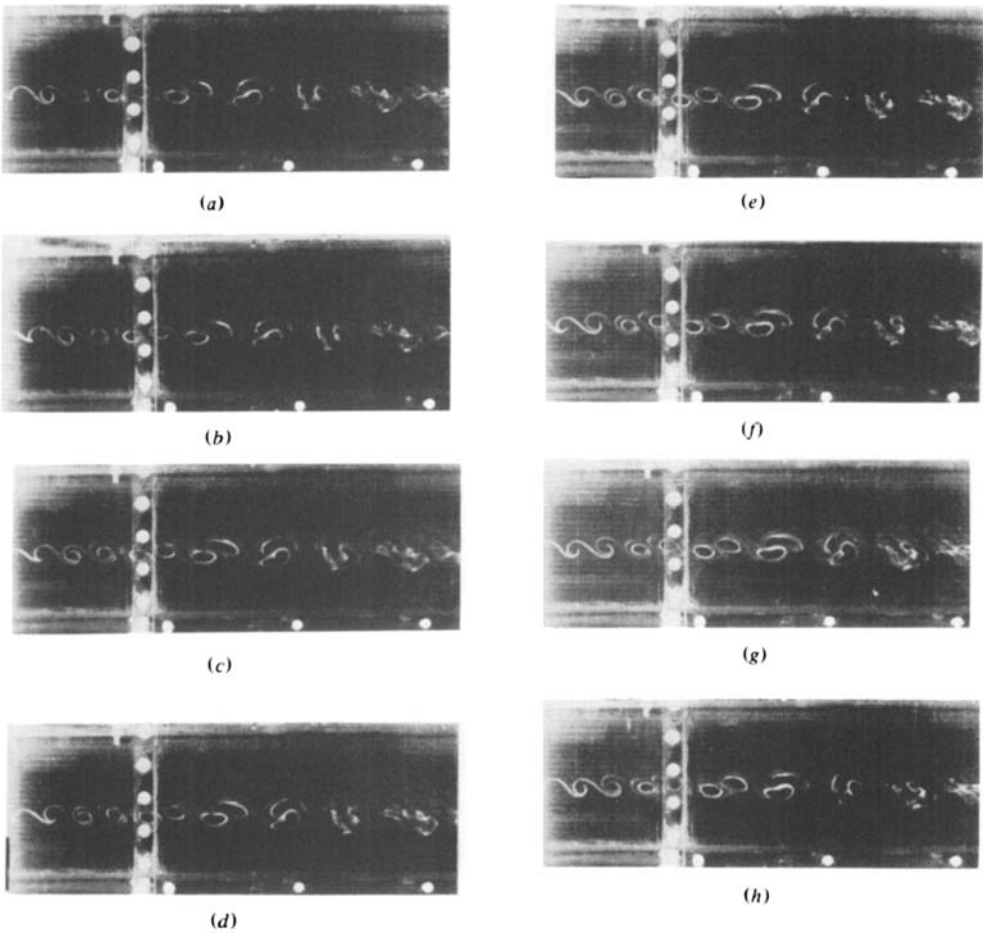

FIGURE 4. Mixing layer under mode II forcing; $f_f/f_m = 0{\cdot}32$, $\Delta\phi = 51{\cdot}4°$.

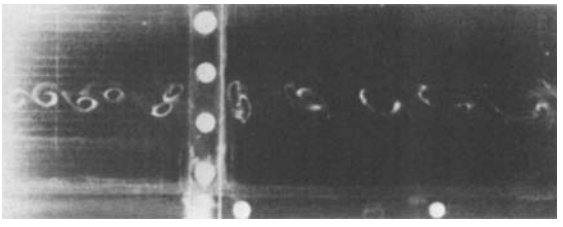

FIGURE 5. Mixing layer under mode II forcing; $f_f/f_m = 0{\cdot}47$.

not forced, the vortices merge randomly in time and in space. The position of the first vortex pairing can be observed at about 15 cm downstream from the trailing edge of the splitter plate. If outside forcing is applied, the location of vortex merging becomes localized. The mixing layer experiences changes when the flow parameters, mean shear, forcing frequency, forcing amplitude etc., vary. Visualization experiments were performed to study the effect of each parameter while other parameters were held approximately constant. Among these parameters the forcing frequency was found to have the most pronounced effect on the mixing layer. The other parameters change the location of the vortex merging, but not the number of vortices in each

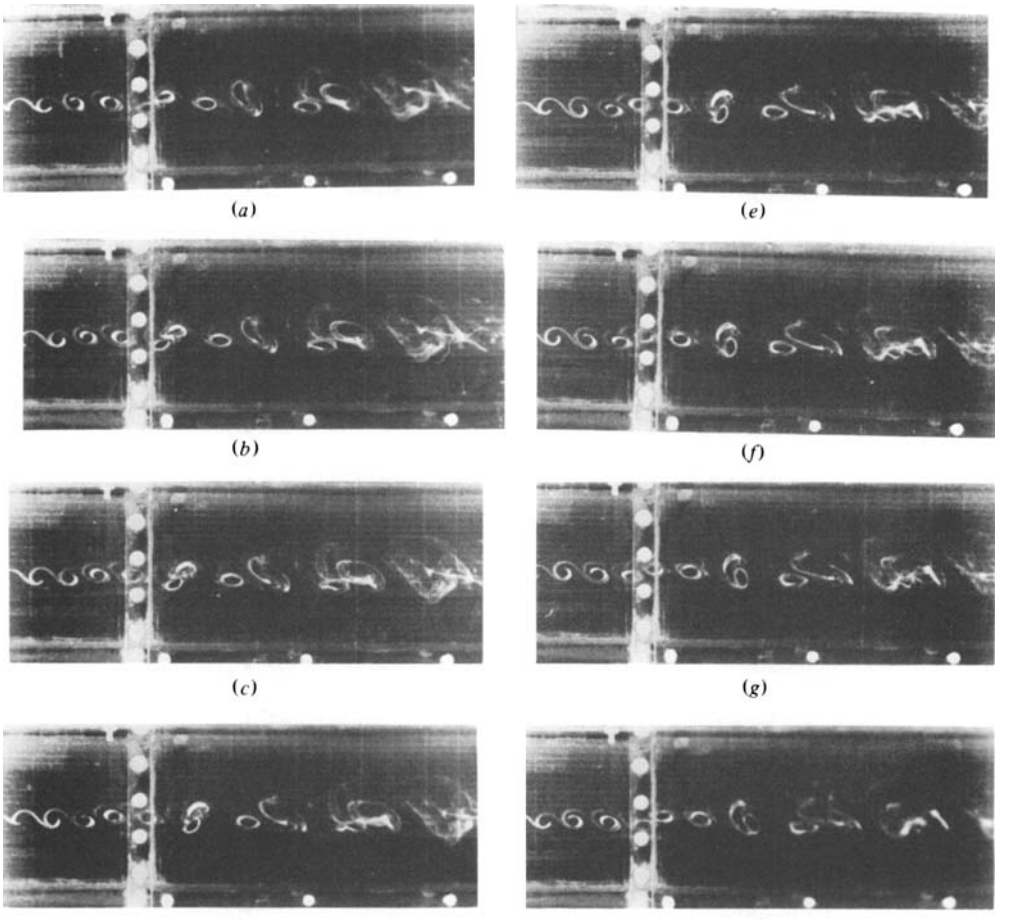

FIGURE 6. Mixing layer under mode III forcing; $f_f/f_m = 0{\cdot}21$, $\Delta\phi = 51{\cdot}4°$.

merging (Ho & Zhang 1981). The effect of variable forcing frequency was studied most extensively.

When the mixing layer is forced in the range of mode I, vortex merging is suppressed for quite a long distance (figure 3). It is clear from the photograph that the suppression of vortex merging inhibits the spreading of the mixing layer. Ultimately, vortex merging resumes and the mixing layer grows further downstream as in the unforced mixing layer. Within the range of mode I, the wavelength at the response frequency, $\lambda_0 = \bar{U}/f_r$ (where $\bar{U} = \frac{1}{2}(U_1 + U_2)$), decreases with increasing forcing frequency, and so does the size of the vortices. The thickness of the mixing layer can be inferred from the wavelength and the size of vortices. Therefore the thickness can be controlled by the forcing frequency. The thickness increases with decreasing forcing frequency until the response frequency switches to mode II. In mode II, every two vortices will merge at a fixed position. Photographs in figure 4 show the evolution of vortices at different phase angles ϕ in a forcing cycle. (In figures 3–8 $\Delta\phi$ is the phase difference between subsequent pictures.) The mixing layer spreads very quickly around the merging position in figure 4, but the thickness stays almost constant until further merging

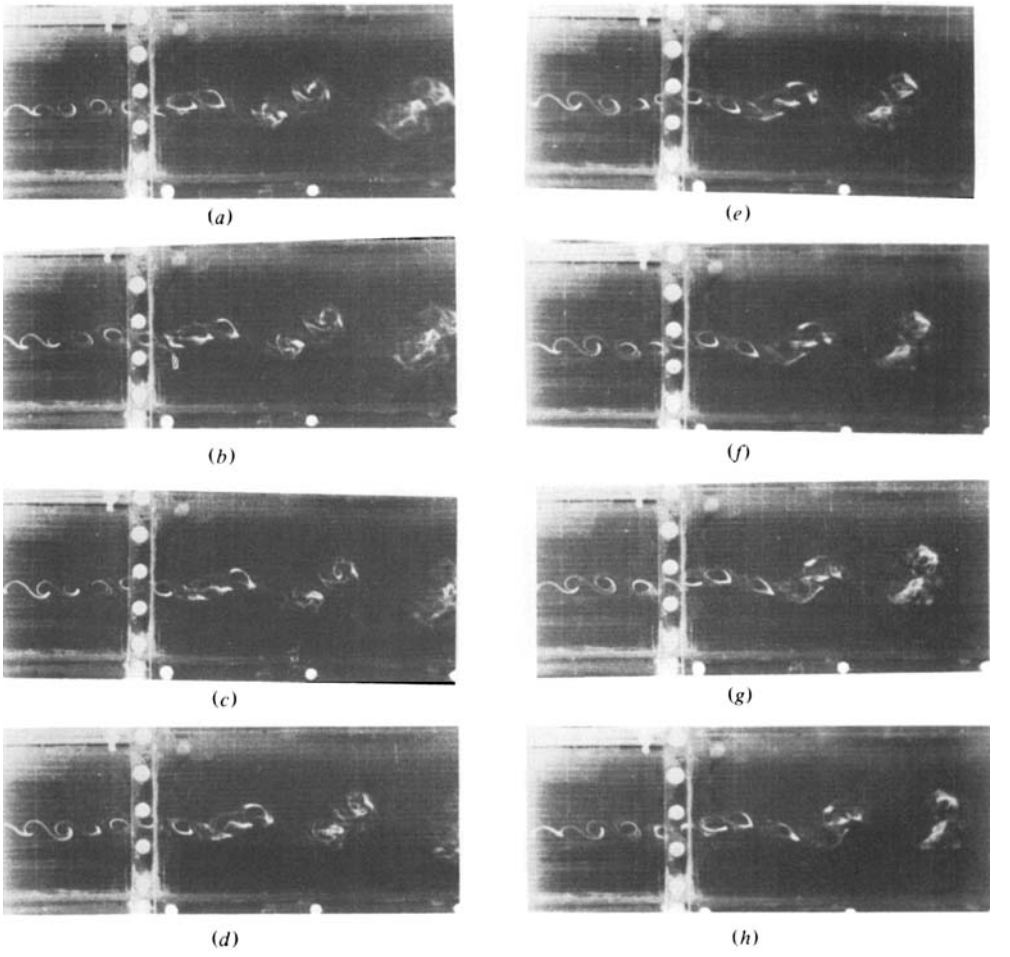

FIGURE 7. Mixing layer under mode IV forcing; $f_f/f_m = 0{\cdot}17$, $\Delta\phi = 51{\cdot}4°$.

takes place. Varying the forcing frequency within mode II also changes the size of the vortices; furthermore, the position of vortex merging moves upstream with increasing forcing frequency (figure 5). With further decrease of the forcing frequency, the response frequency will change to mode III (figure 6), and every three vortices merge together. In mode IV, the merging of four vortices is observed (figure 7). The spreading rate of the forced mixing layer correspondingly increases, and is much larger than that of the unforced mixing layer. In all the modes, it can be observed from these photographs (figures 4–8) that the temporal variation during one cycle of the mixing layer at a certain downstream location is much less pronounced compared with the spatial variation along the mixing layer at one instant. The phase difference between the forcing frequency and the response frequency, i.e. between the subharmonic and the fundamental, can also alter the merging pattern. In most of the mode III tests, two vortices merge first, and the new vortex merges with a third one. For some phase relationships, all three vortices will merge at the same time. In mode IV, two vortices usually merge into a pair, and two pairs then form a single structure. Four vortices merging simultaneously can also be observed at times. Occasionally, three vortices

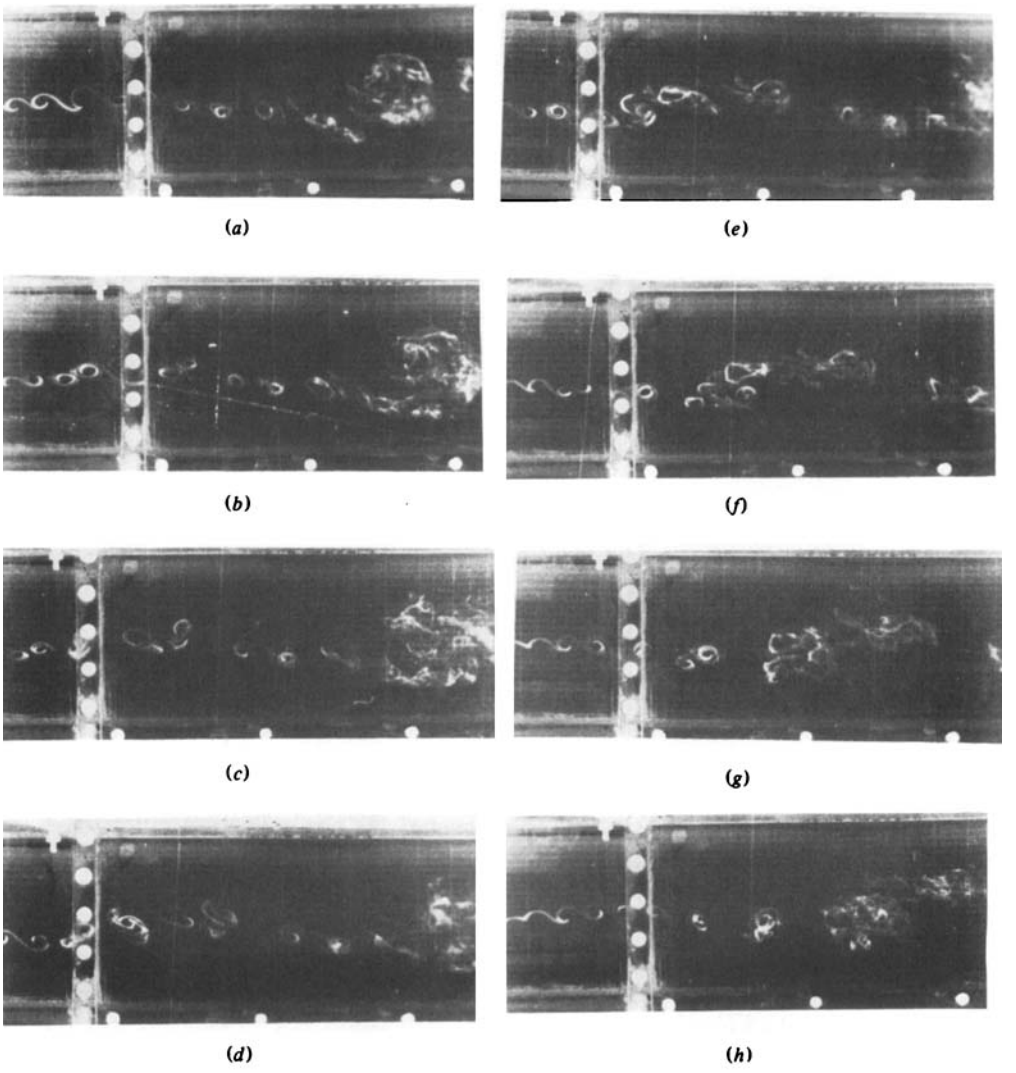

FIGURE 8. Collective interaction; $f_t/f_m = 0{\cdot}1$, $\Delta\phi = 51{\cdot}4°$.

merging simultaneously can be found in an unforced mixing layer. Rockwell (1972) used an external oscillating plate to excite a plane jet. He observed three vortices involved in one merging process. Reynolds & Bouchard (1981) studied a forced axisymmetric jet. They also visualized large spreading of the jet when three vortices merge together.

When the forcing frequency was further decreased and the r.m.s. forcing amplitude at the high-speed side was kept below 0·1 % of $\overline{U}$, the mixing layer behaved like an unforced mixing layer. Well-organized vortex merging did not occur. A very different type of vortex merging was observed when a higher forcing amplitude level was applied (the necessity of high forcing level will be discussed in § 3.3.2). In this case, the vortices initially formed within a wide band near the most-probable passage frequency f_m. The vortices were displaced laterally according to their position, i.e. phase angles, in the cycle of the high-amplitude and low-frequency forcing (figure 8). Owing to

mutual induction and the mean shear (Batchelor 1967) many vortices in one part of the forcing cycle undergo a merging process and form a large turbulent structure, while vortices in other parts of the forcing cycle undergo migration to form a thin region connecting the large structures (Ho & Nosseir 1981). The passage frequency of the resulting coherent structures is equal to the forcing frequency. The phenomenon is called '*collective interaction*'. The high spreading rate and the large drop in the passage frequency are the two characteristics associated with the phenomenon. Collective interaction is a vortex motion governed by nonlinear secondary instability, and was found to be important in many other forced shear layers. Ho & Nosseir (1981) studied an impinging jet with self-sustained oscillations. They found that the collective interaction was a crucial link in the feedback loop. *As a result of the collective interaction, the shear layer contains a single dominant frequency which is an essential characteristic of flows with self-sustained oscillations.* Wygnanski, Oster & Fiedler (1979) forced a mixing layer with a flap at the trailing edge of the splitter plate; the forcing frequency was about one order of magnitude lower than the most-probable passage frequency. The shear layer was observed to have a large spreading rate, and the concept of collective interaction which we introduced here can explain their results. McAlister & Carr (1978) used high-speed ciné films to visualize the flow around a pitching airfoil. An unsteady shear layer appeared above the upper surface, and vortices appeared in the shear layer. The forcing frequency due to the pitching motion is much lower than the vortex-passage frequency. Many small vortices were observed to merge into a single structure, in agreement with the concept of collective interaction.

In the following sections data were measured and reported for mode I, II, III and IV cases. No quantitative results were discussed for the collective-interaction case, because of the extremely large spreading rate and the limited depth of the channel.

3.2. *The initial instability and the formation of vortices*

In this section we will show that the evolution of the various types of vortex merging is dictated by the initial forcing condition and the instability of the mixing layer. This is the reason why even extremely low level forcing can change the mixing layer dramatically.

3.2.1. *The most-amplified frequency.* Near the origin of a free shear layer, the perturbation level is very low. Many experiments have shown that linear stability theory (Michalke 1965) provides good predictions in a jet. For example Freymuth (1966) has shown that the most-amplified frequency and the amplification rate agree with the theoretical results. The phase speeds of the stability waves were determined experimentally by Bechert & Pfizenmaier (1975). However, in a mixing layer some modifications need to be made. Michalke's results are based on the tanh velocity profile with zero velocity on the low-speed side. In this case the velocity ratio R is unity. Huerre (1980) pointed out that the amplification rates at different velocity ratios can be very different owing to the advection effect. Monkewitz & Huerre (1982) performed the stability calculation for various velocity ratios. They found that the most-amplified frequency scales approximately with the maximum slope thickness δ and the average speed $\overline{U}$ of the two streams. The normalized most-amplified frequencies are approximately constant for all velocity ratios. The peak amplification rate increases almost linearly with increasing R. In addition to the effect of the velocity ratio, the mixing

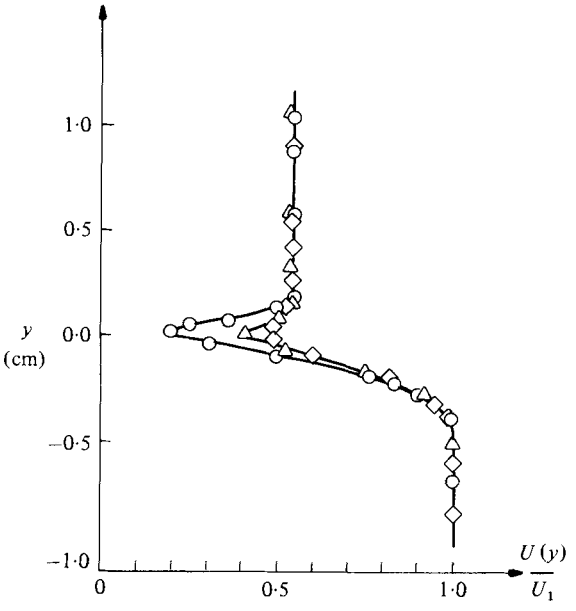

FIGURE 9. Initial development of the mixing layer: ○, x = 0·16 cm; △, 0·80 cm; ◇, 1·43 cm.

layer has another complication; the mean-velocity profile is not well approximated by a tanh profile near the origin. Boundary layers emerge from either side of the splitter plate and form a wake. The development of the mean-velocity profiles is shown in figure 9. Miksad (1972) showed that the presence of the wake did not change the most-amplified frequency, and only affected the amplification rate in the low-frequency region. The most-amplified frequency determines the passage frequency of the coherent structures that govern the dynamics of the mixing layer. In other words, the presence of the wake does not significantly affect the dynamics of the mixing layer. However, Miksad's result was based on a parallel-flow calculation with a non-evolving velocity profile.

Two experiments in the unforced mixing layer were performed to obtain a better understanding of the effect of the wake. In the first one, the speeds of the two streams were kept constant, u_1 = 9·5 cm/s and u_2 = 5·0 cm/s (R = 0·31), so that the thickness of the high-speed side boundary layer was held constant. The thickness of the low-speed-side boundary layer was varied by installing or removing the screen near the trailing edge. The thickness ratio at the low-speed side between the two cases was about 2·6. No appreciable change in the most-probable passage frequency was detected. In the other test, the mean-velocity difference $\Delta U = U_1 - U_2$ was kept the same, but the velocity ratio R was varied. The most probable passage frequency f_m was found to be scaled to the initial momentum thickness θ_0 of the boundary layer on the high-speed side and the average velocity $\overline{U}$ (figure 10). If the summation of the boundary thicknesses θ_0' is used, the normalized frequencies are far from a constant for different velocity ratios (figure 10). Hence the boundary layer on the high-speed side appears to characterize the most-amplified frequency. The boundary layer on the low-speed side does not play an active role. This might be because the high-speed side

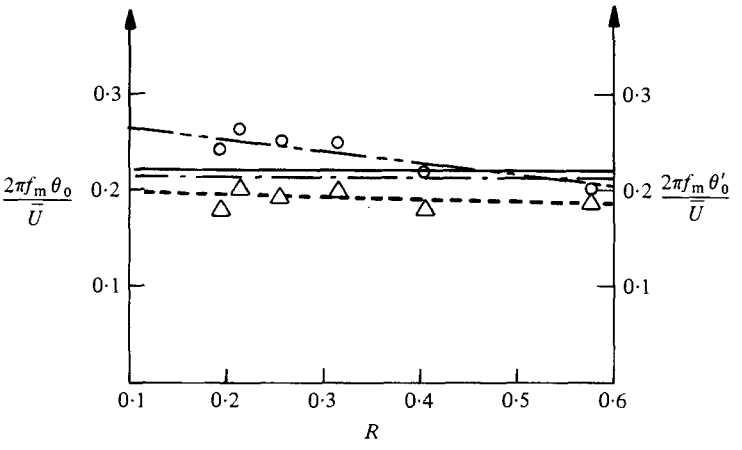

FIGURE 10. The most-amplified frequency: ——, tanh profile; —·—, Blasius profile (Monkewitz & Huerre 1982); —△—, $2\pi f_m \theta_0/\bar{U}$; ··—○··—, $2\pi f_m \theta_0'/\bar{U}$.

shear contains most of the vorticity. Obviously this scaling will not be true for a wake, $R = 0$. However, this method still works for $R = 0{\cdot}2$, which is the smallest velocity ratio tested in the present experiment. Furthermore, the normalized most-probable passage frequency (figure 10) was within a few per cent of the calculated most-amplified frequency f_0, based on the tanh profile or the Blasius profile, i.e. $f_0 \simeq f_m$. The two tests suggest that the length scale in the initial region of the mixing layer should be the thickness of the boundary layer on the high-speed side. The velocity scale is the average speed of the two streams.

3.2.2. *Selection of the response frequency.* In §3.1.1, it was pointed out that the vortices are forming at the response frequency and that several frequency stages can be distinguished. Inside the mixing layer, the level near the response frequency measured by a hot-film probe already dominates the forcing amplitude near the beginning of the mixing layer. The selection of the response frequency by the mixing layer is examined here.

An example of the spectrum outside the mixing layer in mode II forcing is shown in figure 11. The forcing level at the forcing frequency is higher than that of its harmonics, and all of them are barely above the background noise. Inside the mixing layer, the spectrum contains clear sharp peaks both at the forcing frequency and at the response frequency. The r.m.s. values of the streamwise velocity fluctuations $u(f)$ at the forcing frequency and the response frequency are calculated from the spectrum, and the distributions across the shear layer are plotted in figure 12. $u'(f)$ is the normalized value of $u(f)$ ($u'(f) = u(f)/\bar{U}$). Outside the mixing layer, the forcing level on the high-speed side is about one order of magnitude higher than the level on the low-speed side, although the velocity perturbation levels are the same in both compartments at the inlet of the stagnation chamber. The forcing level on the low-speed side is heavily damped by the extra screen installed near the trailing edge of the splitter plate. The normalized velocity fluctuations $u_1'(f)$ at the high-speed side are defined as the forcing levels, and are noted in the figures of different test cases. In both mean streams, the level at the forcing frequency is much higher than the level at the response frequency. Inside the mixing layer, the level at the response frequency

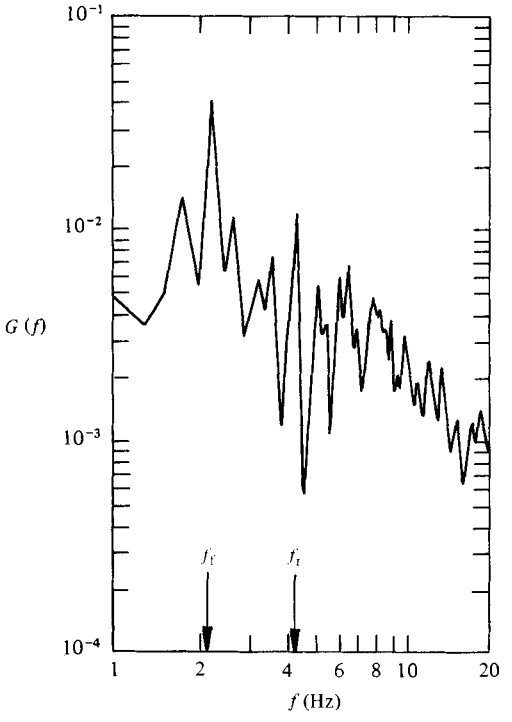

FIGURE 11. A spectrum outside the forced mixing layer; mode II, $f_t/f_m = 0{\cdot}42$, $u_1'(f) = 0{\cdot}10\,\%$, $x = 0{\cdot}16$ cm, $y = -0{\cdot}40$ cm.

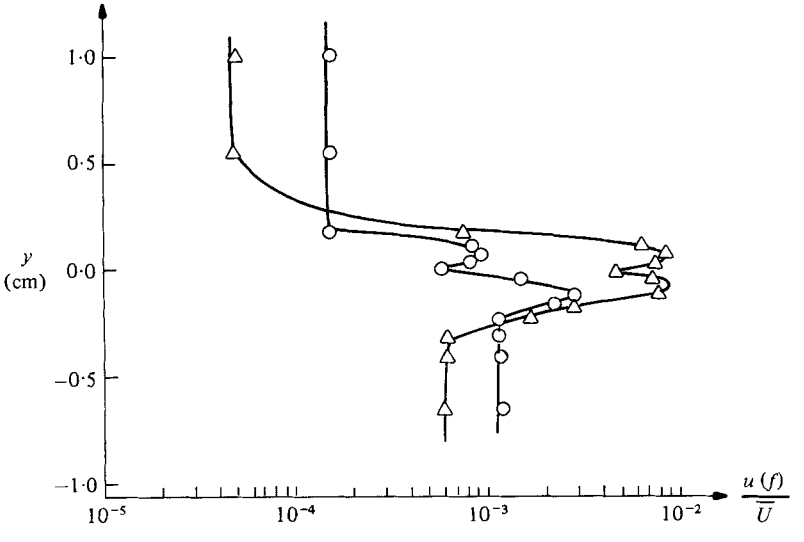

FIGURE 12. The profile of $u'(f)$ across the mixing layer; mode II, $f_t/f_m = 0{\cdot}42$, $x = 0{\cdot}16$ cm. —○—, 2·15 Hz $= f_t$; —△—, 4·30 Hz $= f_r$.

becomes higher than that at the forcing frequency. The result is the same between the first measuring station ($x = 1{\cdot}6$ mm) and the location of the first merging. When the mixing layer is forced in modes II, III, IV, the forcing frequency is rather lower than the most-amplified frequency, one of the harmonics however is closer to f_0 and has a higher amplification rate. This specific harmonic amplifies faster and becomes the

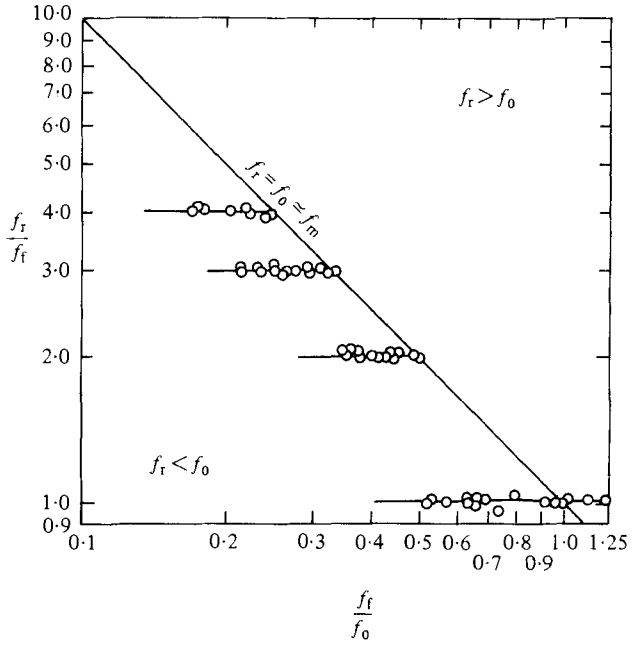

FIGURE 13. The mode diagram.

dominating response frequency in the mixing layer, as shown in figure 12. Further downstream, the vortices evolve from the instability waves and form at the response frequency.

3.3. *Subharmonic and vortex merging*

3.3.1. *The mode diagram.* The relationships among the forcing frequency, the response frequency and the most-amplified frequency having been clarified, another presentation of the data in figure 2 provides the clue to an understanding of the multiple-vortex-merging phenomenon. In figure 13, the ordinate is the ratio of the response frequency to the forcing frequency and the abscissa is the forcing frequency normalized by the most amplified frequency. On the diagonal line, the response frequency equals the most-amplified frequency. Several features pertinent to the forced mixing layer are revealed in this figure. One of the most important characteristics is that the forcing frequency is related to the response frequency through the following equation:

$$f_f = \frac{1}{M} f_r, \tag{1}$$

where M is the mode index and $M = 1, 2, 3, 4$ for modes = I, II, III, IV. Therefore the forcing frequency is the Mth subharmonic of the response frequency at which the vortices form initially in the mixing layer. The integer M is selected by the mixing layer, as described in §3.2.2. This is demonstrated by the fact that all the data are close to the diagonal line where high amplification rates prevail. As the forcing frequency is reduced, the response frequency moves away from the diagonal line, and then switches to a higher mode to stay close to this line, thereby leading to the stages shown on the figure. With the help of (1), the mechanism of the spectacular multiple-

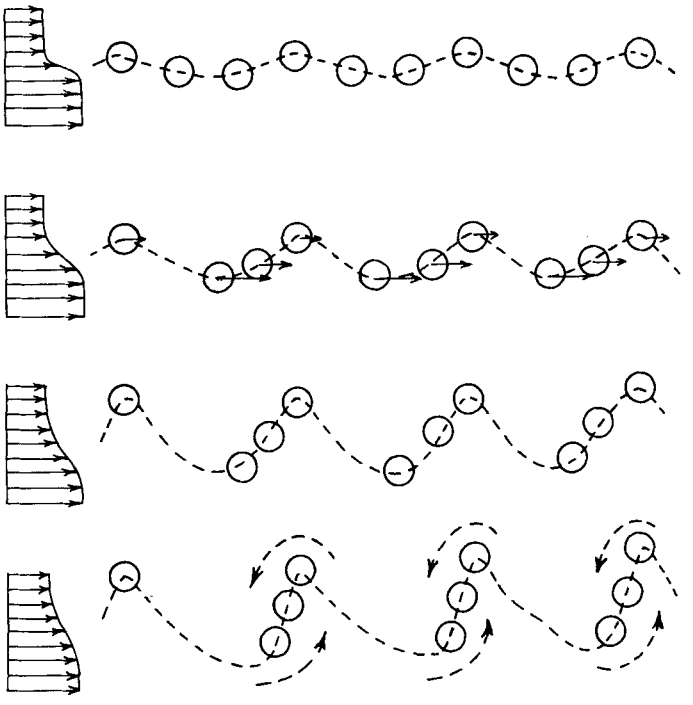

FIGURE 14. Sketch of the multiple-vortex merging.

vortex merging can be explained. In the forced mixing layer, the vortices form at a constant response frequency. A small amount of energy at the forcing frequency, which is exactly the Mth subharmonic of the response frequency, is fed into the mixing layer and amplifies downstream owing to the instability. All the M vortices will then be displaced to different lateral locations according to the individual phase differences between the vortices and the subharmonic (figure 14). Owing to the lateral velocity gradient the vortices will acquire different speeds until M vortices will finally merge into a single structure by kinematic induction. The presence of both fundamental and subharmonic is important for vortex merging. If only subharmonic appears, large vortices will form and no vortex merging occurs (Riley & Metcalfe 1980). In the case of mode I, the initial instability wave is at the forcing frequency that is close to the most-amplified frequency. The subharmonic component is suppressed to an extremely low level when compared with the unforced case because the period and the intensity of the vortices are held constant. The merging is then delayed considerably. Hence one must conclude that the subharmonic of the vortex-passage frequency is an essential element leading to vortex merging.

Another interesting feature in the mode diagram (figure 13) is that the response frequencies are close to the most-amplified frequency, but stay below f_0, except in mode I. The diagonal line in figure 13 is the approximate boundary between the dispersive and non-dispersive regions. This observation reveals that the response frequencies are always dispersive, or at most equal to the most-amplified frequency. However, no plausible explanation is available at present.

3.3.2. *The subharmonic instability.* It has been pointed out in §3.3.1. that vortex merging is formed by the mutual induction of the vortices displaced laterally by

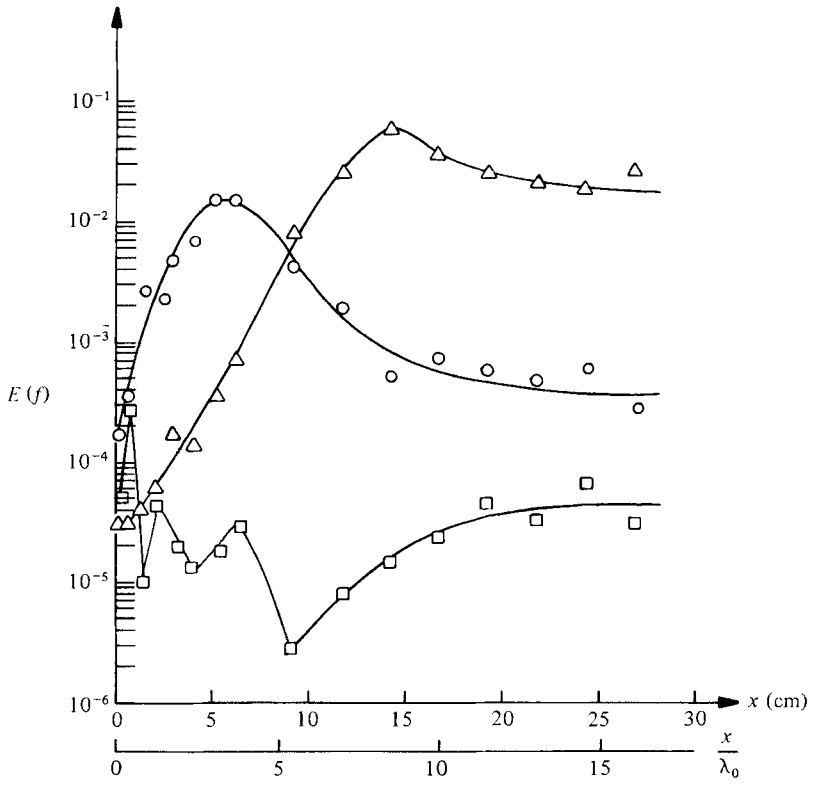

FIGURE 15. Amplification of the energy contents; mode II, $f_t/f_m = 0{\cdot}42$, $u_1'(f) = 0{\cdot}10\,\%$. △—△, 2·15 Hz $= f_i$; ○—○, 4·30 Hz $= f_r$; □—□, 6·45 Hz.

the amplifying subharmonic. A study of the amplification of the subharmonic waves in the mixing layer can clarify many important concepts about vortex merging. Furthermore, although vortex merging has been visually examined; the quantitative description of the phenomenon is somewhat limited (Petersen 1978). In this section, several important concepts are introduced.

The narrow-band velocity fluctuation level $u(f)$ was measured across the mixing layer (an example is shown in figure 12) at many streamwise stations. The normalized values of $u(f)$ were integrated across the mixing layer, and plotted as a function of the streamwise distance. The streamwise energy content is defined as

$$E(f) = \int_{-\infty}^{\infty} \frac{[u'(f)]^2}{2\theta_0} dy.$$

Measurements of $E(f)$ in a mode II mixing layer are shown in figure 15. The energy content at the response frequency reaches a maximum level at $x/\lambda_0 = 4$. From the visualization studies, the instability wave rolls up into a vortex close to the same location. The lateral displacement of the vortices becomes visible near $x/\lambda_0 = 6$, where the streamwise energy contents of the response frequency and of the forcing frequency reach the same level. The spreading rate of the mixing layer increases considerably (figure 25). Several special features occur two wavelengths further downstream at $x/\lambda_0 = 8$ (figure 16):

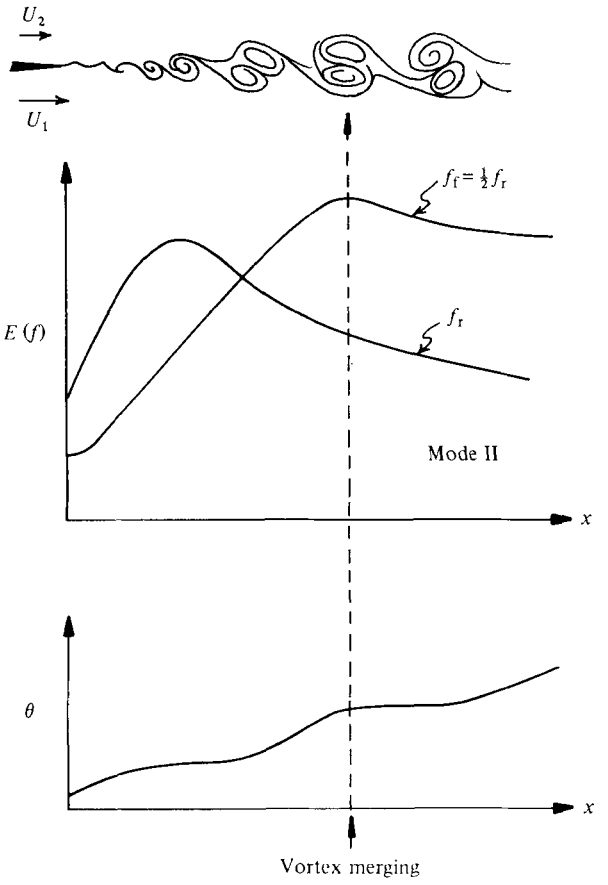

FIGURE 16. The definition of merging location.

(i) the two vortices become laterally aligned from visualization;

(ii) the spreading of the mixing layer stops from this point on until the next merging occurs (figure 25);

(iii) the streamwise energy of the forcing frequency, i.e. the subharmonic, is maximum here.

It is rather subjective to define the exact location of vortex merging, because the merging process is actually accomplished within several wavelengths. However, the three features appearing at $x/\lambda_0 = 8$ seem to characterize the process. Hence we define the position where the subharmonic saturates as the vortex-merging location. *In other words, the vortex merging can be viewed as the subharmonic instability.* When merging occurs, small-scale fluctuations appear, as shown by the dye traces; this can also be inferred from the increased level of the higher harmonics in the spectrum (figure 17). These small-scale fluctuations could be produced by the large strain rate that occurs during merging.

In the mode I case (figure 18), the higher harmonics also increase when merging resumes. It should be noticed that not only is the subharmonic suppressed, but the amplification rate is reduced as well in the non-merging range, as predicted by Riley & Metcalfe (1980). This observation further confirms that the subharmonic is a necessary

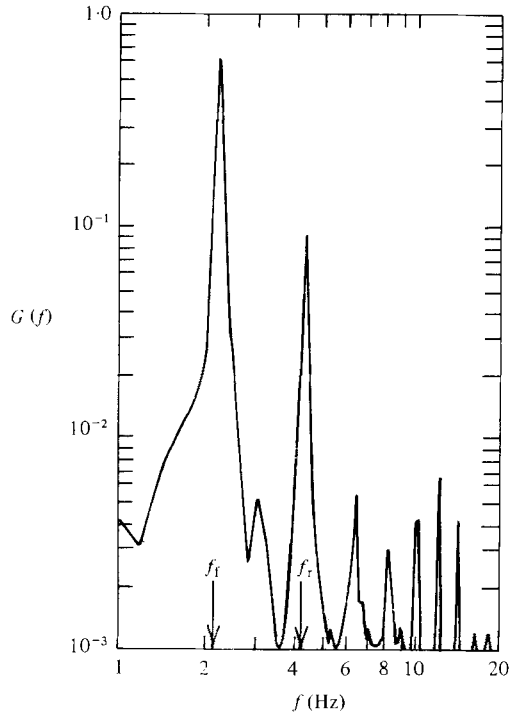

FIGURE 17. Mode II spectrum near the vortex merging; $f_1 = 2{\cdot}15$ Hz, $f_r = 4{\cdot}30$ Hz, $f_1/f_m = 0{\cdot}42$, $u_1'(f) = 0{\cdot}10\,\%$, $x = 16{\cdot}65$ cm, $y = 0{\cdot}1$ cm.

catalyst for vortex merging (figure 14). Similarly to the mode II case, the location of the saturation of the second subharmonic in the mode III case (figure 19) also corresponds to the location where three vortices merge.

In the visualization experiments, it is evident that vortex merging, e.g. modes II, III, IV, is different from the collective interaction due to the substantial difference in required forcing levels. It is expected that the energy content of the forcing frequency will saturate at the position where the vortices coalesce. In the case of collective interaction, the forcing frequency is very low, so the amplification rate is small. With the low forcing level, it takes a long distance for the energy to reach saturation. Usually, before that can happen, some higher-frequency waves (but which are still subharmonics of the response frequency) will amplify faster and reach the saturation level. Thus a relatively small number of vortices coalesce, such that the mixing layer behaves like that of an unforced one. If the forcing level starts from a high value (in the present experiment $u'(f) \simeq 2\,\%$), the energy content at the low forcing frequency can reach the maximum level within a short distance. Then the mixing layer can bypass vortex merging and sustain a collective interaction. The required forcing level for collective interaction should vary with the background noise level at frequencies higher than that at the forcing frequency, and therefore depends on individual experiment. If the forcing level is extremely high and close to the saturating level, the mixing layer can form a large vortex directly.

3.3.3. *The dispersive relation.* The amplification of the subharmonic is pertinent to the vortex merging. Kelly (1967) suggested a subharmonic-resonance mechanism by

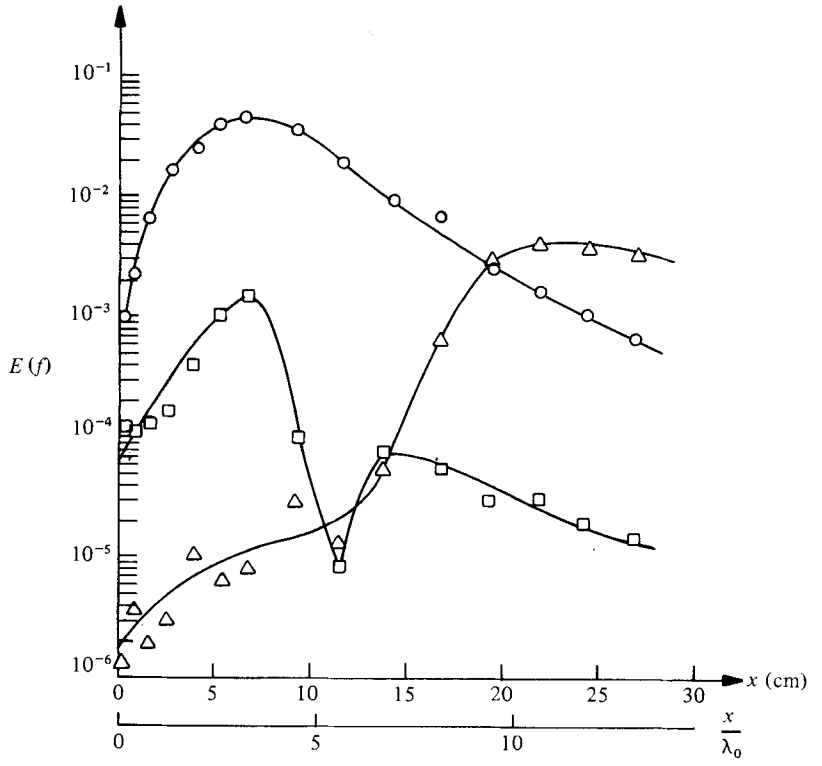

FIGURE 18. Amplification of the energy contents; mode I, $f_t/f_m = 0{\cdot}69$, $u_1'(f) = 0{\cdot}08\,\%$. △—△, 1·75 Hz, ○—○, 3·50 Hz $= f_t = f_r$, □—□, 7·00 Hz.

which the subharmonic can increase its energy through nonlinear interaction. The transfer of energy becomes pronounced when the phased speed of the subharmonic matches the phased speed of the fundamental, i.e. the subharmonic becomes non-dispersive. In a jet, Petersen (1978) found experimentally that the vortices will merge at the location where the subharmonic becomes non-dispersive.

In the mixing layer, the dispersive relation was measured at two locations (figure 20). Very near the origin of the mixing layer ($x = 1{\cdot}3$ cm), the measured dispersion curve agrees well with the theoretical prediction (Monkewitz & Huerre 1982). In a short distance downstream ($x = 3{\cdot}8$ cm), the first subharmonic of the most-amplified frequency f_0 propagates at the same speed as f_0. Hence the subharmonic became non-dispersive near $x = 3{\cdot}8$ cm. The subharmonic takes a fairly long distance to amplify, and reaches the peak at $x = 15$ cm, where the vortices become vertically aligned. In other words, *the non-dispersion of the subharmonic and the vortex merging do not occur at the same location in a mixing layer*. In a jet, the non-dispersion of the subharmonic, however, is an approximation made to identify the merging location. The reason is that the maximum amplification rates of stability waves are much higher in a jet than that in a mixing layer with small velocity ratios. Therefore the locations where the subharmonic becomes non-dispersive, and where it becomes saturated are rather close in a jet.

3.3.4. *The feedback mechanism.* In a mixing layer, Dimotakis & Brown (1976) observed the existence of a long correlation time which could not be scaled with any

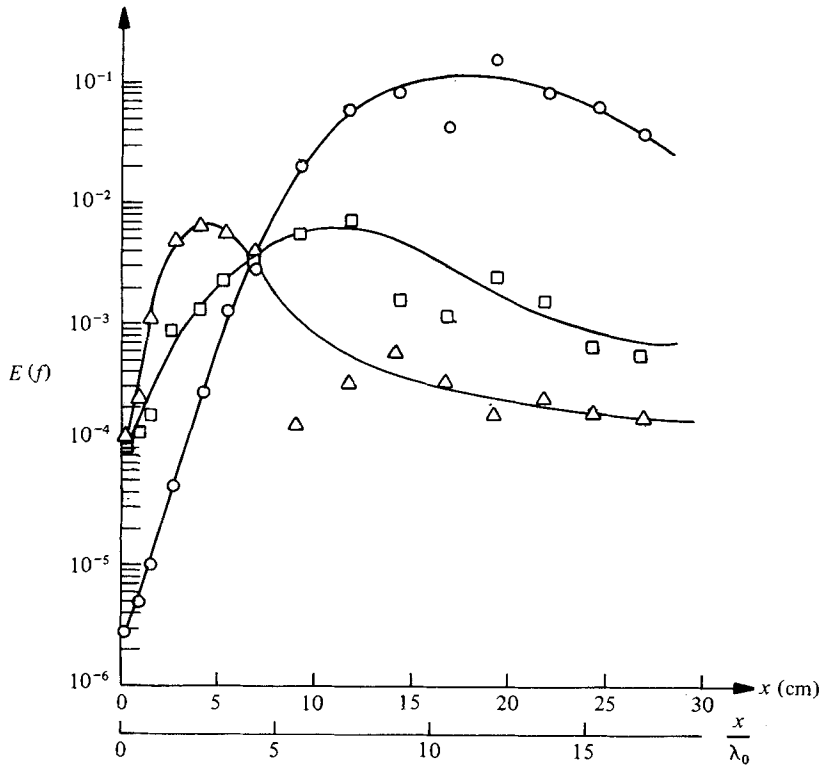

FIGURE 19. Amplification of the energy contents; mode III, $f_t/f_m = 0{\cdot}31$, $u_1'(f) = 0{\cdot}03\,\%$. ○—○, 1·56 Hz = f_t, □—□, 3·13 Hz, △—△, 4·69 Hz = f_r.

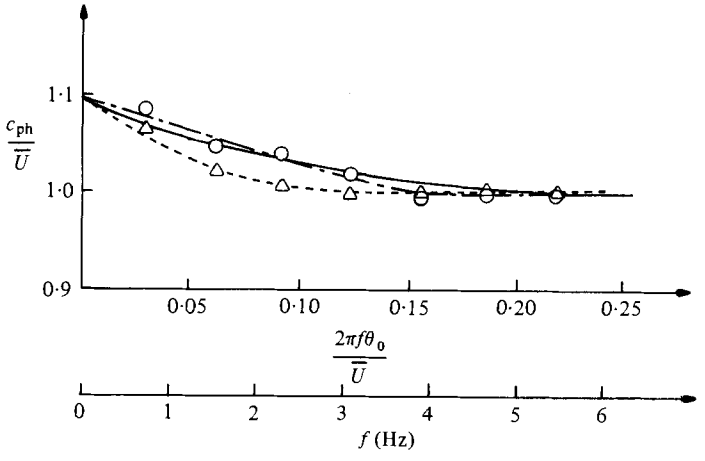

FIGURE 20. The dispersion relation: ○—·—○, $x = 1{\cdot}30$ cm; △---△, $x = 3{\cdot}80$ cm; ——, Monkewitz & Huerre (1982), $R = 0{\cdot}31$.

local flow properties. They proposed that the upstream flow is influenced by the perturbation from downstream through a feedback mechanism. Laufer & Monkewitz (1980) found a low-frequency modulation on the instability wave near the nozzle of a jet. The modulation frequency is about equal to the vortex-passage frequency at the end of the potential core. They suggested that the low-frequency modulation is due

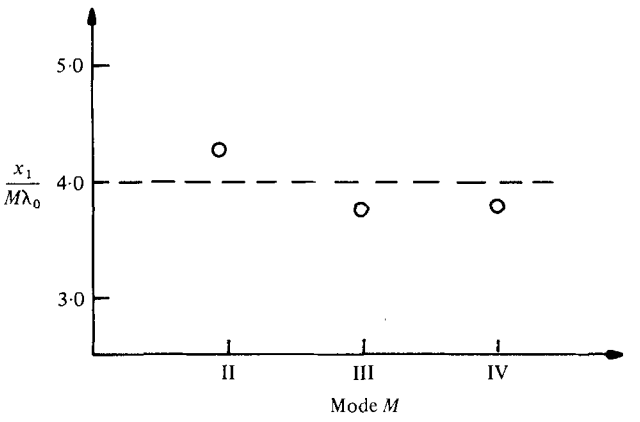

FIGURE 21. Position of vortex merging.

to upstream-propagating flow perturbations produced by the downstream vortex merging and that a feedback loop exists in a free jet, similar to that found in an impinging jet (Ho & Nosseir 1981). They used the same equation developed by Ho & Nosseir to interpret the data in a forced jet (Kibens 1980). The results were found to be satisfactory.

The feedback equation states that the number of waves in a feedback loop should be an integer

$$\frac{x_M}{\lambda_i}+\frac{x_M}{\lambda_a}=N, \tag{2}$$

where x_M is the distance from the trailing edge to the ith merging, and

$$x_M = x_1+x_2+x_3+\dots. \tag{3}$$

x_i is the distance between the $(i-1)$th and the ith merging. λ_i is the wavelength after the ith merging, and λ_a is the wavelength of the upstream-propagating acoustic waves. N is an integer. The equation is derived from the fact that the phase difference between the downstream-travelling waves and the upstream-propagating waves at any point in the feedback loop has to be $2N\pi$, where N is an integer, simply because both wave trains with the same frequency must have the same phase at the same location. One assumption made in deriving (2) is that the downstream phase speed is constant along the paths; otherwise the first term in (2) should be modified.

In the water-channel test, the acoustic wavelength is much larger than λ_i, and the phase speeds are almost constant from the beginning of the mixing layer (figure 20). Equation (2) can be approximated as

$$\frac{x_M}{\lambda_i}=N. \tag{4}$$

For the case of the first merging,

$$\frac{x_M}{\lambda_1}=\frac{x_1}{M\lambda_0}=\frac{f_r x_1}{M\bar{U}}=N, \tag{5}$$

where M is the mode index in (1). This formula explains why the location of merging moves upstream with increasing response frequency in the same mode of forcing, as observed in the visualization experiments (figures 4 and 5). Furthermore, the position

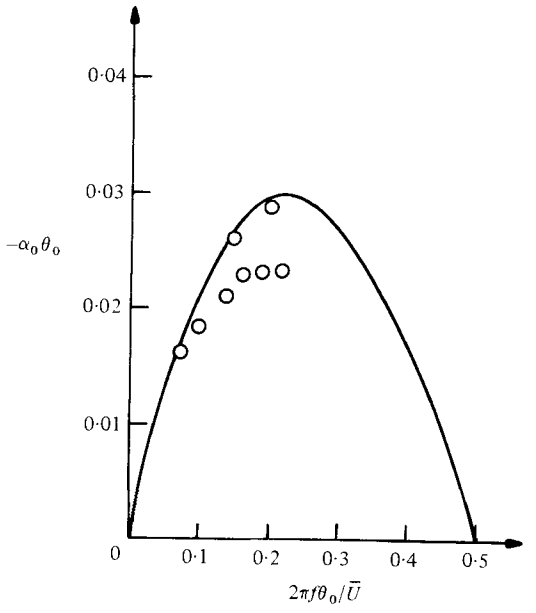

FIGURE 22. The amplification rates; $R = 0{\cdot}31$: ——, Monkewitz & Huerre (1982).

of vortex merging, normalized to the wavelength λ_0 of the response frequency, is found to be constant (figure 21). This result certainly supports the feedback concept (equation (3)).

The feedback idea implies that the location of vortex merging is determined *globally* through (2). The ideas of non-dispersion and saturation of subharmonic depend on *local* conditions only. However, these two mechanisms are not mutually exclusive. *The local stability provides a band of possible frequencies. The global feedback mechanism fine-tunes the mixing layer into a specific frequency according to the feedback equation.*

3.3.5. *The amplification rate and the merging distance.* For a mixing layer with $R = 0{\cdot}31$, the amplification rates at different frequencies were measured (figure 22), and compared favourably with the theoretical result (Monkewitz & Huerre 1982). The stability analysis is an inviscid calculation. In the present case, the Reynolds number $Re = \theta_0 \bar{U}/\nu$, based upon the initial momentum thickness, is only about 31. It is amazing to notice the good agreement. According to the analysis, the maximum amplification rate of instability waves is approximately a linear function of the velocity ratio. The measured value of the maximum amplification rate at $R = 0{\cdot}31$ is about a quarter of the maximum amplification rate for a jet, $R = 1{\cdot}0$.

Equation (4) also provides the location of the first merging, as well as the locations of successive mergings downstream:

$$\left.\begin{aligned} x_1 &= x_2 = NM\lambda_0, \\ x_{i+1} &= 2x_i = NM^i\lambda_0 \quad (i \geqslant 2). \end{aligned}\right\} \tag{6}$$

The value of N in (6) represents the number of subharmonic wavelengths required to accomplish a vortex merging. In the present case, the value of N is 4. For a jet (Gutmark & Ho 1980), the value of N is 2. It appears that the values of N are inversely

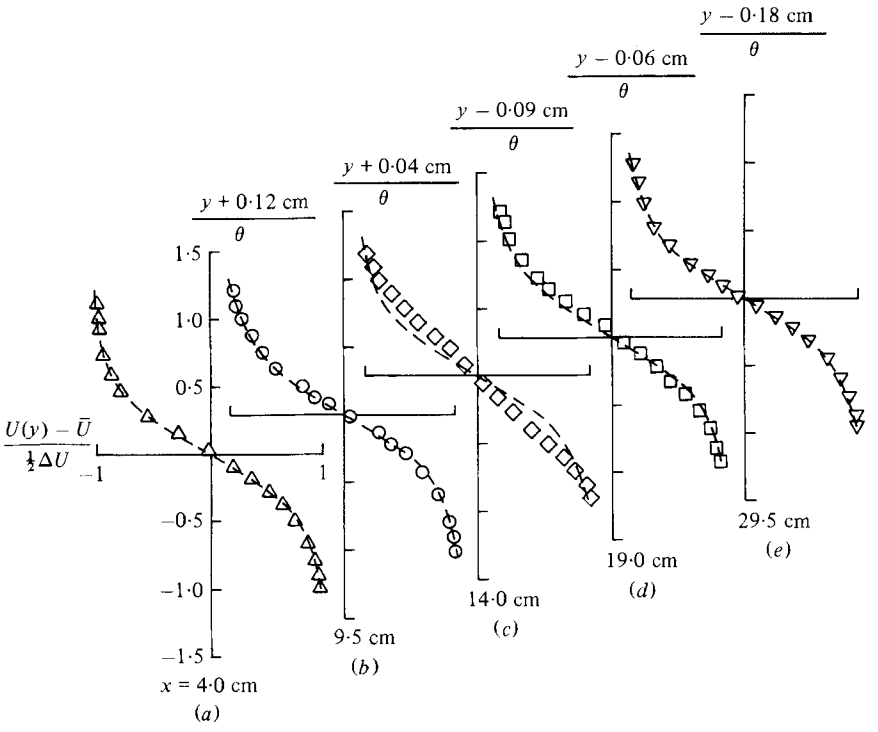

FIGURE 23. The mean velocity profiles of a mode II mixing layer; $f_1/f_m = 0{\cdot}38$, $u_1'(f) = 0{\cdot}09\,\%$. ---, tanh profile.

proportional to the maximum amplification rates at different velocity ratios. Since vortex merging is observed to occur at the climax location of the subharmonic, it is reasonable to expect that the vortices take a longer distance to merge for flow with smaller amplification rate. Consequently, the mixing layer with smaller velocity ratio spreads more slowly (Ho 1981).

3.4. *The development of the forced mixing layer*

3.4.1. *The mean-velocity profiles.* In a forced mixing layer, the shapes of the mean-velocity profiles change with downstream distance. Right after the trailing edge of the splitter plate, two boundary layers merge into a wake flow (figure 9). The wake gradually evolves into a flow with an approximately tanh profile (figure 23*a*, *b*). Further downstream vortices start to merge, the velocity profile shows deviations from the tanh profile due to the vertical movement of the vortices (figure 23*c*). After vortex merging, the velocity profile becomes a tanh profile again (figure 23*d*). The same type of profile occurs in the far-downstream region where random merging takes place (figure 23*e*). In these figures, the vertical axes are normalized as $(y-a)/\theta$, where a is the position where the velocity equals the average velocity $\bar{U}$.

3.4.2. *The spread of the mixing layer.* The momentum thickness θ is used as a measure of the spread. Before the disappearance of the wake, the momentum thickness of the shear layer on the high-speed side is used. The growth of the forced mixing layer is very different from that of an unforced mixing layer (figure 24). The unforced mixing layer first has a parabolic spread due to laminar growth, which is followed by a linear

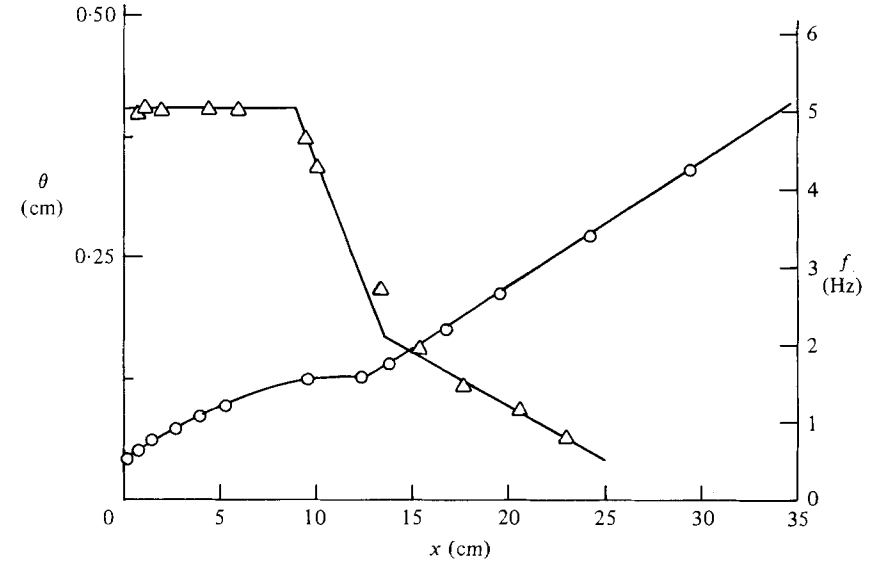

FIGURE 24. The spread of an unforced mixing layer and the vortex passage frequency: △, f (Hz); ○, θ (cm).

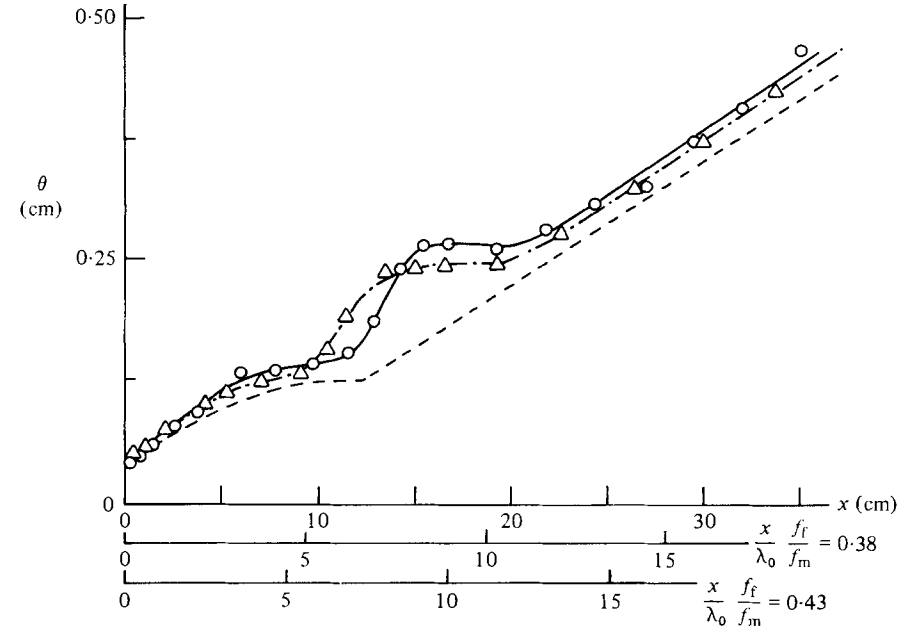

FIGURE 25. The spread of a mode II mixing layer: ○—○, $f_f/f_m = 0{\cdot}38$, $u_1'(f) = 0{\cdot}09\,\%$; △—·—△, $f_f/f_m = 0{\cdot}43$, $u_1'(f) = 0{\cdot}10\,\%$; – – –, unforced mixing layer.

spread due to the random vortex merging in time. The vortex-passage frequency is constant before vortex merging. When vortex merging begins, the frequency decreases linearly with distance. In a forced mixing layer there are regions with stepwise growth due to the localized merging process. An example of a mode II mixing layer is shown in figure 25: the instability wave rolls up into vortices until $x/\lambda_0 = 6$ is reached.

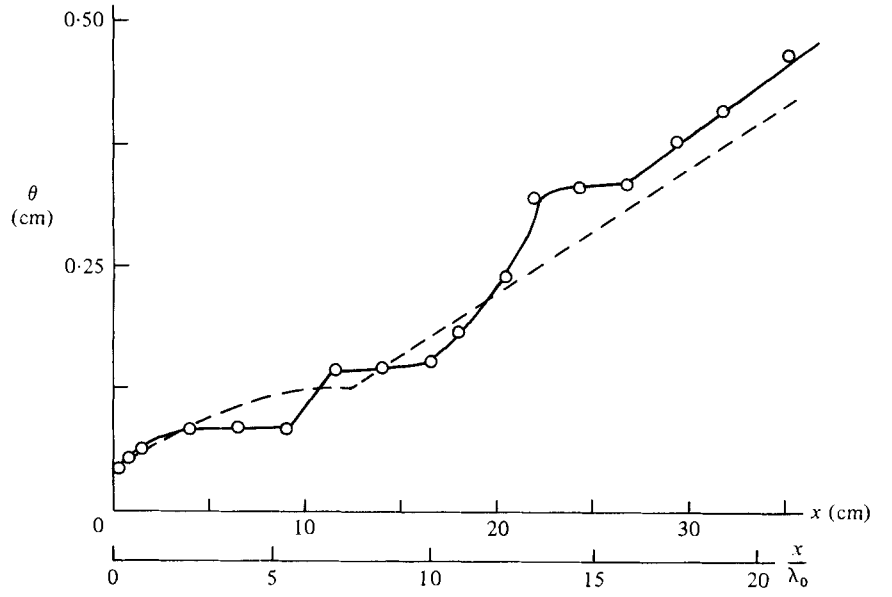

FIGURE 26. The spread of a mode IV mixing layer; $f_t/f_m = 0{\cdot}24$, $u_1'(f) = 0{\cdot}02\,\%$; ———, unforced mixing layer.

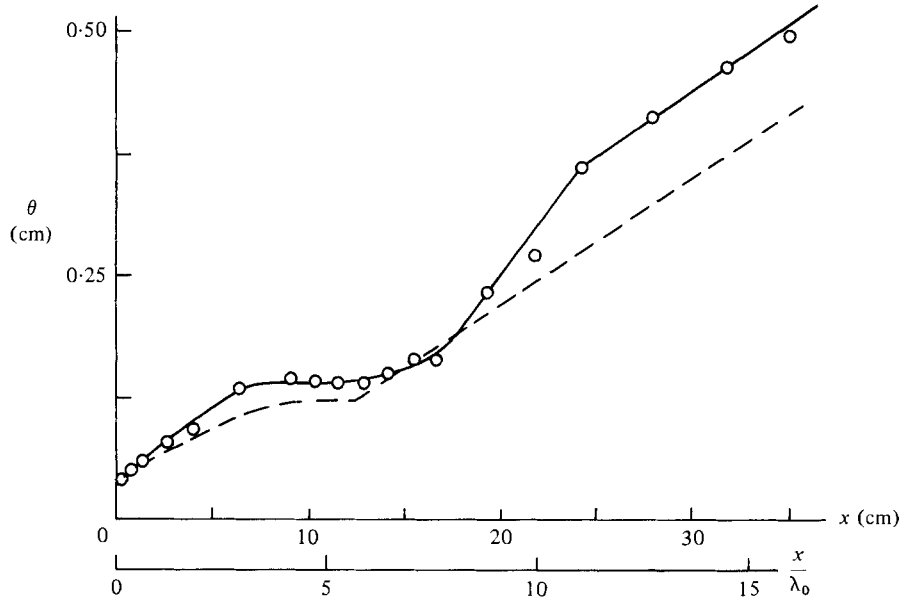

FIGURE 27. The spread of a mode I mixing layer; $f_t/f_m = 0{\cdot}65$, $u_1'(f) = 0{\cdot}07\,\%$; ———, unforced mixing layer.

Beyond this station two vortices start to merge into a single vortical structure. The spreading rate $d\theta/dx$ is very large in this region. Near $x/\lambda_0 = 8$, the merging is completed, and the mixing layer then keeps a constant thickness for an interval. The thickness ratio before and after merging is equal to two. Downstream of $x/\lambda_0 = 12$, merging is not localized any more and the spread becomes linear. In the same mode,

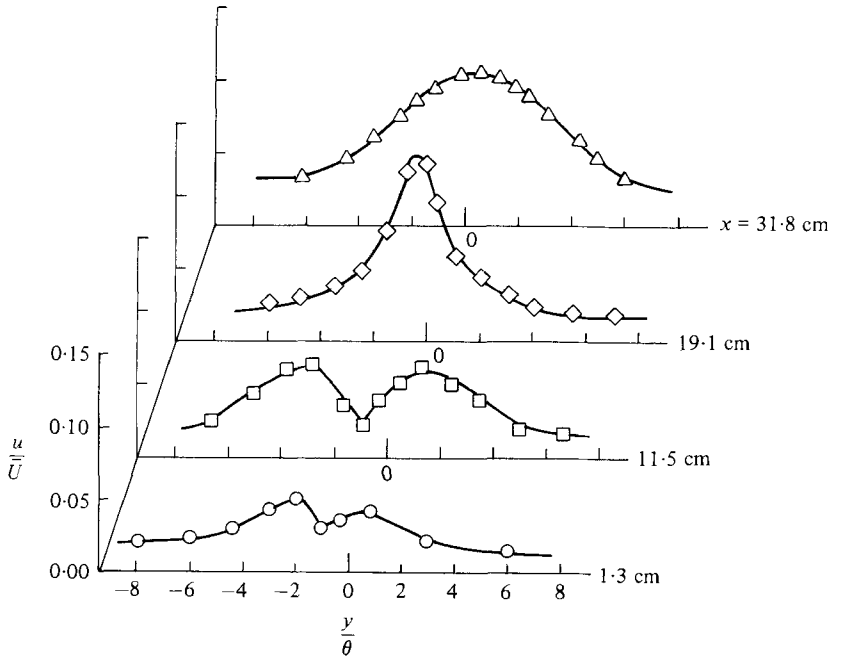

FIGURE 28. The profiles of velocity fluctuations of a mode I mixing layer; $f_1/f_m = 0{\cdot}69$, $u_1'(f) = 0{\cdot}08\,\%$.

it has been observed that the thickness becomes smaller and the merging location moves more upstream (figures 4 and 5), if the forcing frequency is increased. The visualized results are confirmed by measurement in figure 25. In a mode IV mixing layer (figure 26) the first merging is completed also at $x/\lambda_0 = 8$. The difference is the presence of two stages of vortex merging: because the forcing frequency is the second subharmonic of the response frequency, four vortices will ultimately merge together at $x/\lambda_0 = 16$. In mode I (figure 27), the vortex merging is suppressed until $x/\lambda_0 = 8$, and the spreading eventually becomes linear. The asymptotic spreading rates of forced shear layers with different modes have approximately the same value as in the unforced mixing layer. However, the thickness of the mixing layer is different for various modes at the same downstream location. The local thickness and the virtual origin depend on the initial response frequency and the number of mergings already experienced. This is evidence of the long-lasting effect of initial conditions. The importance of the initial condition has been demonstrated by Oster *et al.* (1977), who used an oscillating flap at the trailing edge of the splitter plate and greatly modified the downstream development of the mixing layer. It is also interesting to note that the thickness of the unforced mixing layer close to the leading edge is thinner than that of the forced mixing layer in all modes (figures 25–27). The vortex-passage frequency in an unforced mixing layer corresponds to the most-amplified frequency, which is higher than, or at most equal to, the response frequency in a forced mixing layer (figure 13). The unforced mixing layers have a shorter instability wavelength and a lesser thickness near the origin.

3.4.3. *The level of the velocity fluctuations.* Fluctuating-velocity profiles are very different for various modes. In mode I, vortices do not merge for a long distance.

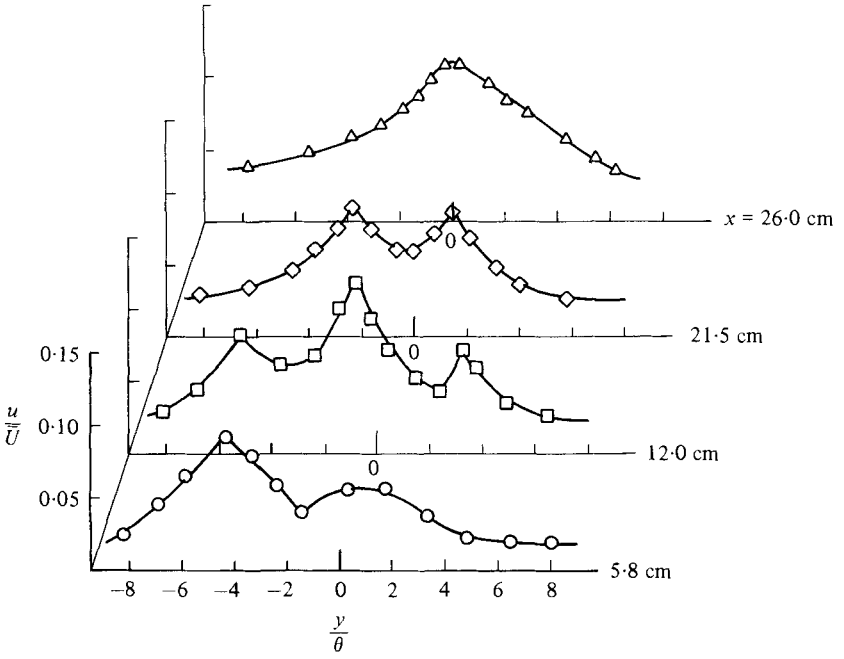

FIGURE 29. The profiles of velocity fluctuations of a mode II mixing layer; $f_t/f_m = 0{\cdot}38$, $u_1'(f) = 0{\cdot}09\,\%$.

Within this range, the streamwise velocity fluctuations have a two-peak profile as the result of a row of well-aligned vortices (figure 28). In the figure, u is the broad-band velocity fluctuation. Far downstream, the peaks are smeared into a single-peak profile where random vortex mergings take place. In a mode II mixing layer, before the first merging, the fluctuating-velocity profile has two peaks (figure 29). At $x/\lambda_0 = 8$, vortices merge, and two vortices are nearly laterally aligned, so that the profile has three peaks. Further downstream, the two vortices form a large vortex, and the two-peak profile characterizing the velocity fluctuations of a single vortex reappears. Finally, the profile has only one peak due to the random merging.

In the experiment by Wygnanski *et al.* (1979), the mixing layer first went through collective interaction, so that many small vortices coalesced into a large vortex. This large vortex will persist for a long distance until its subharmonic amplifies, and makes the large vortex merge again. From this point on, the evolution of the flow is similar to the mode I mixing layer of the present experiment. In both cases the velocity ratios are approximately equal, the spread of the mixing layer reaches a plateau at $x/\lambda_0 = 4$, and the mixing layer starts to grow again at $x/\lambda_0 = 8$. The two-peak profile of the fluctuating velocity also lasts for a long distance in both experiments. Therefore the characteristics of the two experiments are the same in spite of the large differences in Reynolds number. This fact illustrates that the general flow properties are determined by the behaviour of the coherent structures, which are essentially *inviscid* phenomena.

3.5. *Stability theory and the mixing layer*

It has been noticed for some time that many properties in a mixing layer can be calculated from stability theory. For example, Crow & Champagne (1971) used

Mode	f_i/f_m	x (cm)	θ (cm)	$f_i\theta/\bar{U}$	$f_0\theta/\bar{U}$†
II	0·43	0·260	15	0·076	0·079
II	0·38	0·272	18	0·072	0·079
III	0·31	0·329	19	0·071	0·079
IV	0·24	0·336	23	0·056	0·079

† Theoretical neutrally stable frequency; calculation based on tanh velocity profile (Monkewitz & Huerre 1982)

TABLE 1. The normalized frequency at the vortex-merging position

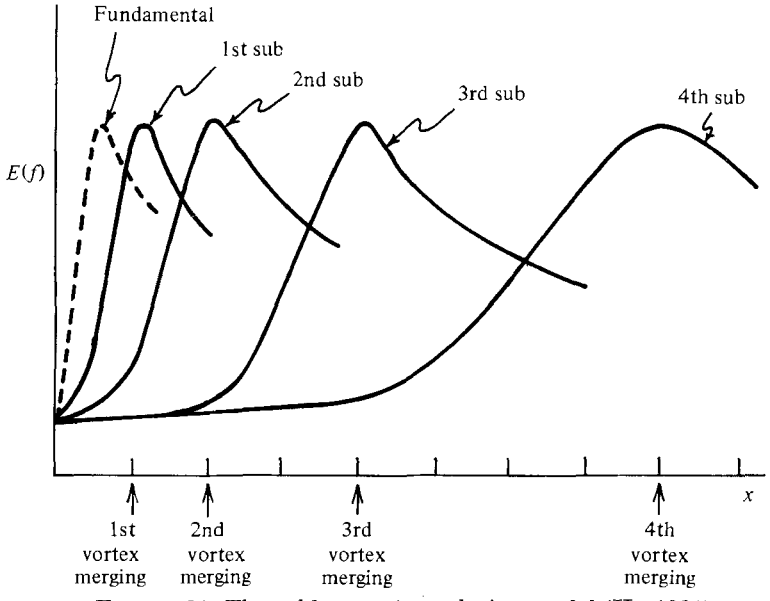

FIGURE 30. The subharmonic evolution model (Ho 1981).

stability analysis to study the preferred mode of an axisymmetric jet. Crighton & Gaster (1976) took the divergence of the jet into consideration, and could calculate the preferred mode based upon the velocity profile at two diameters downstream from the nozzle. Tam (1971) as well as Merkine & Liu (1975) could predict the far-field noise from stability analyses. In the present paper, the evolution of coherent structures is observed to have close relationship with the stability analyses. However, it is generally accepted that the vortex merging, the preferred mode and the noise generation involve highly nonlinear process. It is then a paradox that the properties of nonlinear flow can be predicted from linear stability theories.

This experiment suggested that the subharmonic can be viewed as a catalyst of the vortex merging. A further examination of the subharmonic leads to an explanation of the abovementioned paradox. In the unforced mixing layer, more than two vortices are only occasionally involved in a merging. Hence we will limit our discussion to an examination of this case. At the location where the subharmonic reaches its peak, the vortex merging occurs, and the local thickness doubles (figure 25). If the subharmonic frequency is normalized with the local momentum thickness at its peak and the average

speed, then the normalized frequency is equal to the neutrally stable frequency based upon linear theory (table 1). Furthermore, the ratio between the neutrally stable frequency and the most-amplified frequency is about two (Monkewitz & Huerre 1982). Hence, whenever vortex merging occurs, *the change of local length scale* makes the original subharmonic become neutrally stable, and the new subharmonic become the most amplified wave (figure 30).

Based upon this observation, a model termed 'subharmonic evolution' was proposed by Ho (1981). One major assumption made in the model is that the normalized amplification rate of the ith subharmonic equals the linear amplification rate:

$$\alpha_i \theta_i = \alpha_{i+1} \theta_{i+1} = \alpha_0 \theta_0 \quad (i \geqslant 2). \tag{7}$$

Many of the characteristics of the mixing layer in the nonlinear region, e.g. the preferred mode, the distance between merges, the spreading rate and the flight effect of noise generation, can then be derived from the model (Ho 1981). It becomes clear that the linear stability analyses should *not* be directly applied to the downstream region where the nonlinear effect prevails. However, the infinite stages of newly evolved subharmonics make the direct use of linear stability analyses *appear* to work.

For a mode II flow (figure 15), the amplification rate of the subharmonic equals the linear amplification rate. However, more experimental data are needed to substantiate the assumption. Recently, Pierrehumbert & Windnall (1982) studied a subharmonic wave superimposed on a row of vortices. They found that the amplification rate is not sensitive to the distribution of the vorticity, and is approximately equal to the linear amplification rate. This result provides additional support for the subharmonic evolution model.

4. Conclusion

In the present experiment, a subharmonic forcing technique has demonstrated the capability of greatly manipulating the vortex merging. With very low forcing level, several vortices can merge simultaneously and dramatically change the spreading rate. A large number of vortices can also coalesce together through the collective interaction which is different from the ordinary vortex merging. A high forcing level is required.

In a forced mixing layer, the initial formation of the vortices depends on the stability process and the external forcing function. The vortices form at the response frequency, which is one of the harmonics of the forcing frequency, and is close to the most-amplified frequency. The interaction between the fundamental, the response frequency, and the Mth subharmonic, the forcing frequency, leads to the merging of M vortices. The merging is very much delayed if the subharmonic is suppressed by forcing the shear layer near its most-amplified frequency. Hence the presence of the subharmonic is necessary in vortex merging. Furthermore, the subharmonic starts to amplify long before the vortices change their lateral position significantly, and begins to decay where the vortex merging is completed. Therefore the subharmonic should be viewed as the *catalyst* instead of the *product* of the vortex merging.

The locations of vortex merging can be predicted from the feedback equation. The distance between mergings is inversely proportional to the velocity ratio. The evolution of the coherent structures in a mixing layer appears to be controlled by the *global feedback mechanism*, and the *local stability*.

In the case of merging of two vortices, which is the most common situation in an unforced mixing layer, the momentum thickness doubles where vortex merging is completed. The change of the local length scale makes the 'old' subharmonic evolve from amplifying local subharmonic to decaying local fundamental, and a 'new' subharmonic becomes the most amplified wave. From this experimental evidence, a model of subharmonic evolution is proposed, and can explain many of the characteristics of a mixing layer. Strictly speaking, linear stability theory should *not* be applied to the region where nonlinearity prevails. However, at each stage, the regenerated subharmonics grow with the same rate as the linear amplification rate, and the linear stability calculation *appears* to be able to predict some phenomena produced by nonlinear mechanisms.

The authors would like to express their appreciation to Professors J. Laufer, F. K. Browand and P. Huerre for their useful discussions. This work was supported by the Office of Naval Research.

REFERENCES

Acton, E. 1976 *J. Fluid Mech.* **76**, 651.

Ashurst, W. T. 1976 *Bull. Am. Phys. Soc., Ser.* II. **21**, 1428.

Batchelor, G. K. 1967 *An Introduction to Fluid Dynamics*. Cambridge University Press.

Bechert, D. & Pfizenmaier, E. 1975 *J. Fluid Mech.* **72**, 341.

Browand, F. K. & Weidman, P. D. 1976 *J. Fluid Mech.* **76**, 127.

Brown, G. L. & Roshko, A. 1974 *J. Fluid Mech.* **64**, 775.

Crow, S. C. & Champagne, F. H. 1971 *J. Fluid Mech.* **48**, 567.

Corcos, G. M. & Sherman, F. S. 1976 *J. Fluid Mech.* **73**, 241.

Crighton, D. G. & Gaster, M. 1976 *J. Fluid Mech.* **77**, 397.

Dimotakis, P. E. & Brown, G. L. 1976 *J. Fluid Mech.* **78**, 535.

Fiedler, H. E. 1980 Initiation, evolution and global consequences of coherent structures in turbulent shear flows. In *Proc. Symp. on Coherent Structures, Madrid, Spain.*

Freymuth, P. 1966 *J. Fluid Mech.* **25**, 683.

Gutmark, E. & Ho, C.-M. 1980 Feedback mechanism in a free jet. *Bull. Am. Phys. Soc., Ser.* II. **25**, 1102.

Ho, C.-M. 1981 Local and global dynamics of free shear layers. In *Proc. Symp. on Numerical and Physical Aspects of Aerodynamic Flows*. Springer.

Ho, C.-M. & Huang, L.-S. 1978 *Bull. Am. Phys. Soc., Ser.* II. **23**, 1007.

Ho, C.-M. & Nosseir, N. S. 1981 *J. Fluid Mech.* **105**, 119.

Ho, C.-M. & Zhang, Y. Q. 1981 On the manipulation of spreading rate of mixing layers. In *Proc. 3rd Int. Symp. on Turbulent Shear Flows, University of California, Davis.*

Huerre, P. 1980 *Phil. Trans. R. Soc. Lond.* A **293**, 643.

Kelly, R. E. 1967 *J. Fluid Mech.* **27**, 657.

Kibens, V. 1980 *A.I.A.A. J.* **18**, 434.

Kim, H. T., Kline, S. J. & Reynolds, W. C. 1971 *J. Fluid Mech.* **50**, 133.

Knight, D. D. 1979 Numerical investigation of large scale structures in the turbulent mixing layer. In *Proc. 6th Biennial Symp. on Turbulence, University of Missouri, Rolla.*

Kovasznay, L. S. G., Kibens, V. & Blackwelder, R. F. 1970 *J. Fluid Mech.* **41**, 283.

Laufer, J. & Monkewitz, P. 1980 *A.I.A.A. Paper* no. 80-0962.

Merkine, L. & Liu, J. T. C. 1975 *J. Fluid Mech.* **70**, 353.

McAlister, K. W. & Carr, L. W. 1978 *NASA* TM-78446.

Michalke, A. 1965 *J. Fluid Mech.* **23**, 521.

Miksad, R. W. 1972 *J. Fluid Mech.* **56**, 695.

MONKEWITZ, P. & HUERRE, P. 1982 The effect of the velocity ratio on the spatial stability of a 2-D mixing layer. *Phys. Fluids.* (to appear).

OSTER, D., WYGNANSKI, I., DZIOMBA, B. & FIEDLER, H. 1977 On the effect of initial conditions on the two dimensional turbulent mixing layer. In *Proc. Symp. on Turbulent Flow, Berlin.*

PIERREHUMBERT, R. T. & WIDNALL, S. E., 1982 The two- and three-dimensional instabilities of a spatially periodic shear layer. *J. Fluid Mech.* **114**, 59.

PETERSEN, R. A. 1978 *J. Fluid Mech.* **89**, 469.

REYNOLDS, W. C. & BOUCHARD, E. E. 1981 The effect of forcing on the mixing layer region of a circular jet. In *Proc. IUTAM Symp. on Unsteady Turbulent Shear Flows.* Springer.

RILEY, J. J. & METCALFE, R. W. 1980 *A.I.A.A. Paper* no. 80-0274.

ROCKWELL, D. O. 1972 *A.S.M.E. Paper* no. 72-WA/APM-21.

TAM, C. K. W. 1971 *J. Fluid Mech.* **46**, 757.

WINANT, C. D. & BROWAND, F. K. 1974 *J. Fluid Mech.* **63**, 237.

WYGNANSKI, I. & FIEDLER, H. E. 1970 *J. Fluid Mech.* **41**, 327.

WYGNANSKI, I., OSTER, D. & FIEDLER, F. 1979 A forced plane turbulent mixing layer: a challenge for the predictor. In *Proc. 2nd Symp. on Turbulent Shear Flow, Imperial College, London.*